Colloids and Surfaces A: Physicochemical and Engineering Aspects 700 (2024) 134767

Contents lists available at ScienceDirect

Colloids and Surfaces A: Physicochemical and Engineering Aspects

journal homepage: www.elsevier.com/locate/colsurfa

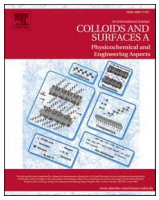

Effect of a fluorinated surfactant on Langmuir monolayer properties of minimal-linker gemini surfactants

Srikant Kumar Singh [1], Matthew F. Paige [2,*]

Department of Chemistry, University of Saskatchewan, 110 Science Place, Saskatoon, SK S7N 5C9, Canada

GRAPHICAL ABSTRACT

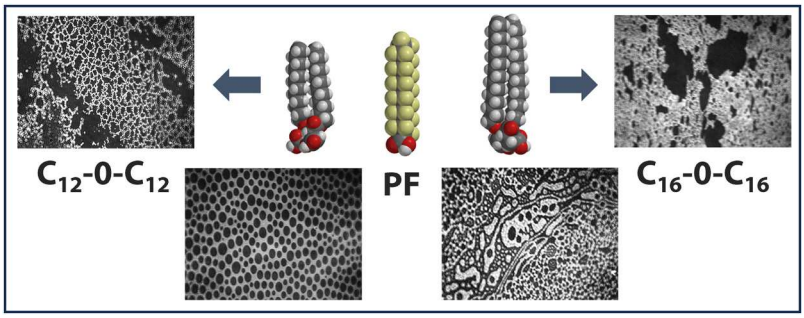

ARTICLE INFO

Keywords:
Interfacial mixing
Dimeric surfactants
Perfluorotetradecanoic acid, Langmuir monolayers, binary surfactant mixtures, gemini surfactants

ABSTRACT

A new class of carboxylic acid-terminated gemini surfactants which contain the smallest possible headgroup linker (a single bond) has recently been reported in the literature. In this current work, we have explored how Langmuir monolayers of two different alkyl tail chain length variants (n = 12, n = 16) of these surfactants, dubbed C_n-0-C_n, are impacted by mixing with a benchmark perfluorinated surfactant, perfluorotetradecanoic acid (PF). Pure PF and C_{16}-0-C_{16} monolayers share similar general characteristics, yielding compact, incompressible, solid-like films at the air-water interface. In contrast, the shorter tail chain variant, C_{12}-0-C_{12} forms expanded, compressible liquid-like films. While both tail chain variants formed mixed films with PF that were generally expanded in comparison with their pure components, and were also phase-separated, the extent of interactions between film components and the resulting micron-scale morphology of the mixed films were different for the two alkyl chain lengths. Overall, PF induces different packing behavior in both the systems and the observations are attributed to the difference in the dispersion forces originating from the tail chain length differences.

* Correspondence to: Department of Chemistry, University of Saskatchewan, Saskatoon, SK S7N 5C9, Canada
E-mail addresses: srikant.singh@usask.ca (S.K. Singh), matthew.paige@usask.ca (M.F. Paige).
[1] https://orcid.org/0000–0001-5678–4228
[2] https://orcid.org/0000–0002-5552–8123

https://doi.org/10.1016/j.colsurfa.2024.134767
Received 16 April 2024; Received in revised form 12 June 2024; Accepted 6 July 2024
Available online 8 July 2024

1. Introduction

The development of novel, new surface-active amphiphilic molecules is of ongoing interest to the surfactant community. Gemini surfactants, which contain two hydrophilic head groups linked by a spacer and two hydrophobic tail groups, typically offer superior performance properties to their corresponding monomeric analogs, including lower critical micelle concentrations (CMCs), orders of magnitude higher surface-activity and the ability to self-assemble into unique and useful aggregates. [1–5] Synthetic efforts have yielded an enormous variety of gemini surfactants with different chemical structures to date and readers are directed to reviews on this topic. [2,6–14] Of particular interest has been exploring the role played by the chemical structure of the spacer group as this has been found to be highly-impactful on surface activity; the spacer can be hydrophilic or hydrophobic, flexible, or rigid, heteroatomic, aromatic, leading to a wide range of surfactant characteristics. [2,6,15–21] Of recent importance has been a newly developed group of carboxylic acid-based gemini surfactants (C_n-0-C_n; n = # of carbon atoms in tail chains; Fig. 1A and B) which have the smallest possible linker (a single covalent bond). These compounds, sometimes referred to as surfactants with a "minimal linker" are synthetically tractable and, in our view, represent a useful extreme reference point in assessing how the chemical structure of gemini linkers impact surfactant performance. These compounds are well-suited to assess fundamental air-water interfacial properties such as surfactant packing, film morphology and intermolecular interactions through Langmuir monolayer investigations.

Intermolecular interactions between perfluorinated and hydrogenated surfactants in mixed monolayers are of significant recent interest in the literature. Mixtures of these surfactants in monolayers typically yield highly-structured, phase-separated films, although the extent of mixing and the resulting micron and nanometer length-scale phase-separated morphologies that form in these systems is a strong function of surfactant chemical structure; for a recent review, see ref. [22] The most well-studied mixed monolayer systems are simple binary mixtures of fatty acids with perfluorinated fatty acids. Complex domain structures can be generated through balancing attractive forces within the phase-separated hydrogenated phase, primarily through dispersion forces which scale with tail chain length, with net repulsive interactions between the non-polarizable perfluorinated tails and the hydrocarbon tails at domain boundaries. We have recently reported that C_{18}-0-C_{18} behaves akin to a dimeric fatty acid, including its ability to form phase-separated, highly-crystalline films with a benchmark perfluorocarbon. [23,24] Thus, it is clear that the C_n-0-C_n family of compounds provides a useful test subject for further systematic assessment of structure-mixing relationships.

In the current work, we have investigated mixed perfluorocarbon—C_n-0-C_n monolayers, where n = 12 and n = 16. A few of the bulk surfactant properties, including CMC, surface tension, phase behavior, foam stability, and interfacial rheology have been explored in detail for C_{12}-0-C_{12} and its mixtures with other surfactants in different media. [25–28] These reports broadly note that the minimal spacer imparts relatively low structural flexibility to the molecule and that this significantly impacts its interfacial properties. Acharya et al. have measured very low CMC values for C_{12}-0-C_{12} (8.9×10^{-5} M by surface tension and 5.0×10^{-5} M by the fluorescence-probe method) [25] which is orders of magnitude lower than the monomeric analog (2.5×10^{-3} M). [29] The authors have also explored its synergistic effect of lowering the CMC of mixtures with sodium dodecyl sulfate (SDS). Further, the SDS–C_{12}-0-C_{12} mixture displayed better foam stability and foam properties than either of the individual solutions. [25] Villa et. al. have studied four different tail chain variants (with n = 8, 10, 12 and 14) to understand their behavior in aqueous medium and found that the CMC values of the C_n-0-C_n molecules decrease with decreasing number of carbon atoms in the alkyl chains up to n = 12. [28]

While we are unaware of major studies that have focused on properties of C_{16}-0-C_{16}, we have reported on fundamental characteristics of C_{18}-0-C_{18} monolayers in pure films and films mixed with a benchmark perfluorinated fatty acid, perfluorotetradecanoic acid ($C_{13}F_{27}COOH$; PF, shown in Fig. 1D). [24] Pure C_{18}-0-C_{18} monolayer films were close-packed and formed highly-ordered crystalline films that shared similar characteristics to simple fatty acid monolayers. In mixed monolayers, C_{18}-0-C_{18} and PF mixed non-ideally, attributed to the repulsive interactions between the hydrophobic tails of the gemini surfactant and the non-polarizable perfluorinated tails of the PF, with the films exhibiting phase-separation. [23,24]

Herein, we further explore the impact of chemical structure on mixing properties of the C_n-0-C_n class of compounds with PF by characterizing films prepared from C_{12}-0-C_{12} and C_{16}-0-C_{16}. As the only difference between these variants and the previously reported C_{18}-0-C_{18} is tail chain length, we posit that any differences in mixing behavior for the variants will be driven by differences in attractive dispersion forces between the hydrogenated component of the mixed films. Thus, we hypothesize that mixed films with C_{16}-0-C_{16} will tend towards greater

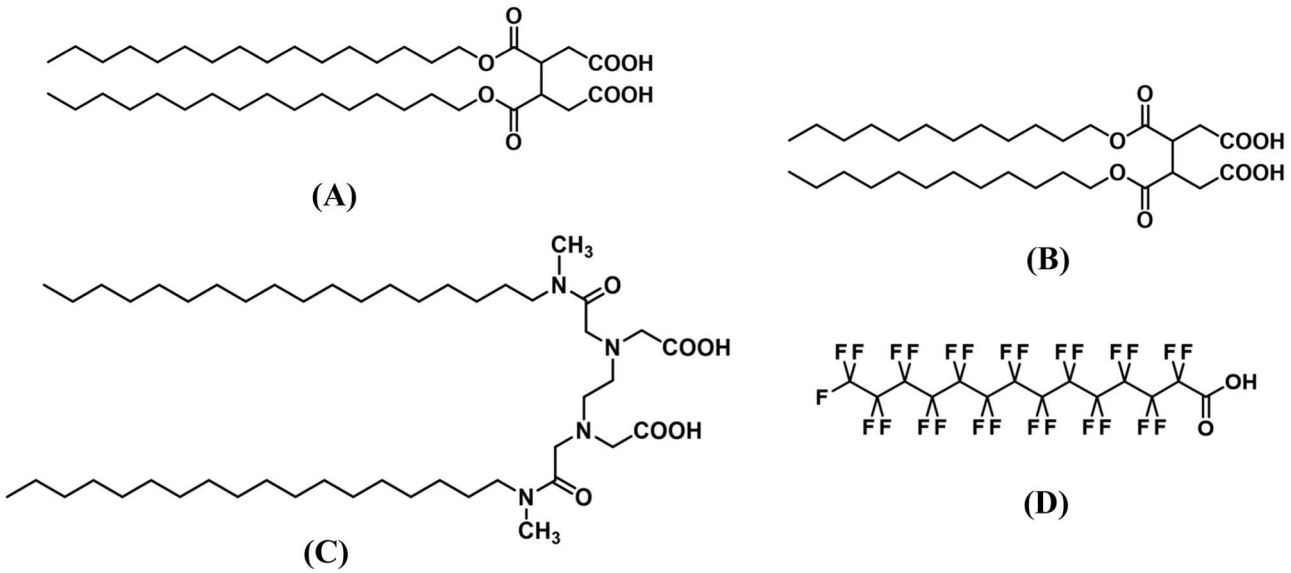

Fig. 1. Expanded chemical structures of **(A)** C_{16}-0-C_{16}, **(B)** C_{12}-0-C_{12}, **(C)** Ace[18]-2-Ace[18], and **(D)** Perfluorotetradecanoic Acid surfactants.

level of compaction and phase-separation whereas this will occur to a lesser degree for the shorter chain gemini surfactant. The results of experiments involving surface pressure-area isotherms and film morphology using Brewster Angle Microscopy are reported and discussed, below, in context of simple fatty acid comparators and other affiliated gemini surfactants reported in the literature.

2. Materials and methods

2.1. Materials

C_{12}-0-C_{12} was kindly supplied by Chukyo Yushi Co. Ltd., Japan. The received sample was further purified by recrystallization either from toluene or hexane/ethyl acetate. The synthetic scheme, purification and characterization procedure for C_{16}-0-C_{16} has been adapted from ref. 23 using 1-hexadecanol as the alcohol. PF (purity 96 %) was purchased from Sigma-Aldrich and used without further purification. Stock solutions of C_n-0-C_n were prepared in chloroform (1 mM) and that of PF was prepared in 9:1 hexanes:THF mixture. Chloroform (> 99.8 %) and hexanes (> 98.5 %) were obtained from ThermoFisher Scientific. Tetrahydrofuran (THF; ≥ 99.9 %) was procured from Millipore Sigma. All the solvents involved were ACS grade or better. For mixed solutions of C_n-0-C_n and PF, film compositions are described in terms of the molar ratios of PF:C_n-0-C_n using the notation X:Y.

2.2. Monolayer film preparation and characterization

Langmuir films of C_n-0-C_n, PF and their mixtures were prepared on a Langmuir trough (Biolin KSV) filled with ultrapure water (Barnstead, resistivity = 18.2 MΩ·cm^{-1}) subphase. The surface pressure was measured with a Wilhelmy balance using a filter paper plate. The two barriers enabled symmetric (lateral) compression of the film at a rate of 20 mm^2·min^{-1} (approximately 5.0 Å^2 molecules·min^{-1}). Blank runs were recorded to ensure a clean subphase surface. The surfactant solutions (100 μL) were then spread onto the clean subphase using a Hamilton syringe, and the films were compressed after ~ 15 minutes equilibration time to allow for film stabilization and solvent evaporation. Three replicate isotherms were performed for each mixture to confirm reproducibility, with film areas varying by less than ±1.0 Å^2·molecule^{-1}. All measurements were carried out at 22 ± 1 °C. For Brewster Angle Microscopy (BAM), the films were illuminated by a 658 nm laser using an UltraBAM microscope (KSV Biolin) equipped with a camera, operating at an acquisition rate of 20 frames·s^{-1}.

3. Results and discussions

3.1. Compression isotherms and film compressibility

Information on surfactant packing at the air-water interface was obtained from surface pressure−molecular area (π−A) compression isotherms and their corresponding compressibility modulus plots ($C_s^{-1} = -A(d\pi/dA)_T$ vs π), with isotherms for the three pure films shown in Fig. 2 A. The area occupied by the films at the onset of intermolecular contact can be assessed through the "lift-off" mean molecular area, estimated from where the isotherm begins to increase sharply. For the three pure films, the most compact film was PF (lift-off ~ 30 Å^2/molecule), followed by C_{16}-0-C_{16} (~55 Å^2/molecule) and then by C_{12}-0-C_{12} (~110 Å^2/molecule). As expected, PF occupies a much smaller area at the interface than the dimeric gemini surfactants, by virtue of its considerably smaller monomer headgroup area. The area of C_{16}-0-C_{16} is approximately double that of PF and comparable with the previously reported C_{18}-0-C_{18}, [23] which adsorbs normal to the water surface at higher film compressions and, as noted above, effectively behaves as a dimeric fatty acid. Maximum compressibility modulus values for PF and C_{16}-0-C_{16} were similar (~ 300 mN/m, values which are typically taken to indicate a solid film [30]) indicating the two compounds formed monolayer films of similar rigidity.

The only difference in molecular structure between C_{12}-0-C_{12} and C_{16}-0-C_{16} is the length of the tail chain, and thus our working hypothesis to explain the difference in interfacial packing area is that the shorter tail-chain length of C_{12}-0-C_{12} results in lower dispersion forces between molecules, thus resulting in a significantly more expanded film. The expanded, featureless isotherm for C_{12}-0-C_{12} observed here bears a close resemblance to those which we have reported previously for a different class of gemini surfactants, Ace(n)-2-Ace(n) with n = 12, 18, with chemical structure of Ace[18]-2-Ace[18] shown in Fig. 1C. [31,32] These compounds yielded amorphous, liquid-phase films due to their sterically bulky head groups that impeded them to close-pack into crystalline, solid films at the air-water interface. While care must be taken in extrapolating results from Ace(n)-2-Ace(n) compounds to C_{12}-0-C_{12} systems due to their structural differences, empirical trends gleaned until this point suggest that C_{12}-0-C_{12} forms similar non-diffracting film (see Figure S1, Supporting Information) that is liquid in nature. This was confirmed by the Grazing-incidence X-Ray Diffraction (GIXD) measurements for the C_{12}-0-C_{12} film (results described in SI). While we currently lack corresponding GIXD data for C_{16}-0-C_{16} films, we hypothesize that C_{16}-0-C_{16} monolayers closely

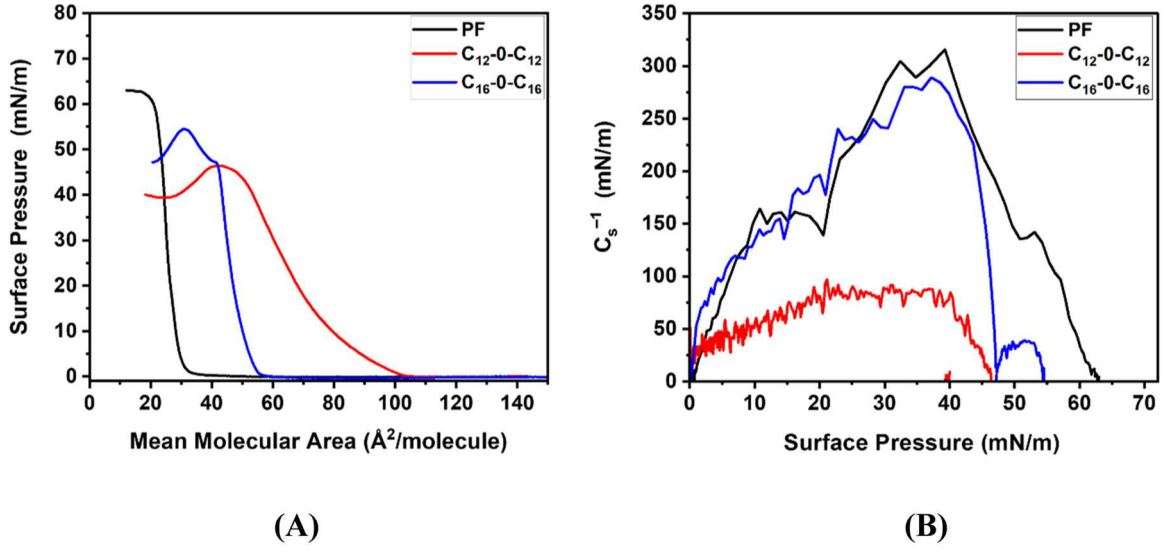

Fig. 2. **(A)** Isotherms and **(B)** compressibility modulus plots of pure PF, C_{12}-0-C_{12} and C_{16}-0-C_{16} films.

resemble those of C_{18}-0-C_{18} [23] because of several similarities reported later in this work (vide infra). Further, film compressibility modulus values for C_{12}-0-C_{12} were overall smaller than those for C_{16}-0-C_{16}. Emblematic of this is the lower $C_{s\max}^{-1}$ value for C_{12}-0-C_{12} which was typical for a compressible, liquid-like film. The impact of the chain difference length and the resulting micron-scale film morphology will be examined later in the manuscript.

For the mixed films of C_n-0-C_n with PF, we first consider isotherms for the mixed C_{12}-0-C_{12}-PF system, shown in Fig. 3 A. For PF-dominant and equimolar mixtures (4:1, 2:1, 1:1), a clear phase transition around the collapse pressure of pure C_{12}-0-C_{12} films (~ 47 mN/m) was observed, with the transition indicated with an arrow in the accompanying compressibility plot for the equimolar mixture (Fig. 3B). The compressibility plots for the rest of the mixed films have been included in Supporting Information (SI, Figure S2).

For the C_{12}-0-C_{12} dominant mixtures (1:2, 1:4), there were no such phase transitions detected and the isotherms were, except for being expanded, comparable with pure C_{12}-0-C_{12} films. The overall shape of the isotherms resembled that of pure C_{12}-0-C_{12}. We also note that the two films show a surface pressure plateau that stretches until the physical limit of compression in our trough, with no signs of a "conventional" collapse pressure. Even with larger spreading volumes, we did not see a conventional film collapse under any conditions, suggesting the mechanism of film collapse is strongly dependent on composition in these systems. For the discussion below, we treat these mixtures as having collapse pressures comparable to pure C_{12}-0-C_{12} (~ 50 $Å^2$/molecule).

Collectively, this behavior is typically observed when the less surface-stable film component, in this case C_{12}-0-C_{12}, is squeezed out of the monolayer and into the subphase. This is typically taken as a characteristic of an immiscible (phase-separated) mixture upon application of the "two-dimensional" phase rule first proposed by Defay and Crisp. [33,34] The Defay-Crisp analysis enables systematic monitoring of the collapse pressure for a phase change in one or both film components as a function of film composition, with an ideally miscible system following relation 1 (represented by blue-dashed line in Fig. 4 A):

$$\pi_{12} = \pi_1\chi_1 + \pi_2\chi_2 \quad (1)$$

A completely immiscible system will not follow this ideal law, but will yield instead a flat, horizontal plot (green dotted line; Fig. 4 A) showing no deviation from the collapse pressures of the pure components. Any deviations from the ideal law suggests non-ideal mixing of the two components, as displayed by the trend for the C_{12}-0-C_{12}—PF mixtures: the higher collapse pressures closer to the PF's collapse pressure dominate until 1:1 composition, after which, the films show lower collapse pressures closer to the pure C_{12}-0-C_{12} film.

The application of Defay-Crisp analysis is limited by several factors such as the monolayers not being in a state of equilibrium during film collapse and the collapse pressure complications for the higher C_{12}-0-C_{12} mixing ratios noted above. Thus, the analysis needs to be supplemented with additional information. To further assess interactions within the mixed films, additivity plots (mixed film area as a function of composition) are shown in Fig. 4B. The ideal behavior predicted from the additivity relationship for fully immiscible (or fully mixed) films is given by Eq. (2)[35]:

$$A_{12} = A_1\chi_1 + A_2\chi_2 \quad (2)$$

where A_{12} is the area for the binary mixed film, A_n is the area of the film for component n, and χ_n is the mole fraction of component n. Deviations in experimental data from Eq. 2 is indicative of either repulsive (in the case of positive deviations) or attractive (in the case of negative deviations) interactions between film components. At the surface pressures examined, the additivity plots generally showed modest positive deviations from ideal mixing, indicating net repulsive interactions between the film components and that the mixed films were more expanded than predicted by Eq. 2. The extent of these deviations became smaller for all compositions at higher surface pressures, and for one composition (4:1) at the highest pressure (40.1 ± 0.4 mN/m), small negative deviations were observed. We speculate that this anomaly is attributed to this surface pressure being close to the phase transition observed for the 4:1 mixture at which C_{12}-0-C_{12} is pushed out of the monolayer, though the precise nature of the interactions remains unclear.

The extent of the interactions can be further represented by excess Gibbs free energies of mixing (ΔG_{ex}) plotted as a function of surface pressure for the mixed films given by Eq. (3). [35]

$$\Delta G_{Ex} = \int_0^{\pi} [A_{12} - (\chi_1 A_1 + \chi_2 A_2)]\, d\pi \quad (3)$$

where again, A_{12} is the area per molecule of the mixed film, A_n is the area of the pure film and χ_n is the mole fraction of the pure components. The mixed systems yielded positive values of excess Gibbs free energy (films destabilized relative to ideality) for all compositions at the four examined surface pressures, with values ranging from ~ 391 J·mol^{-1}

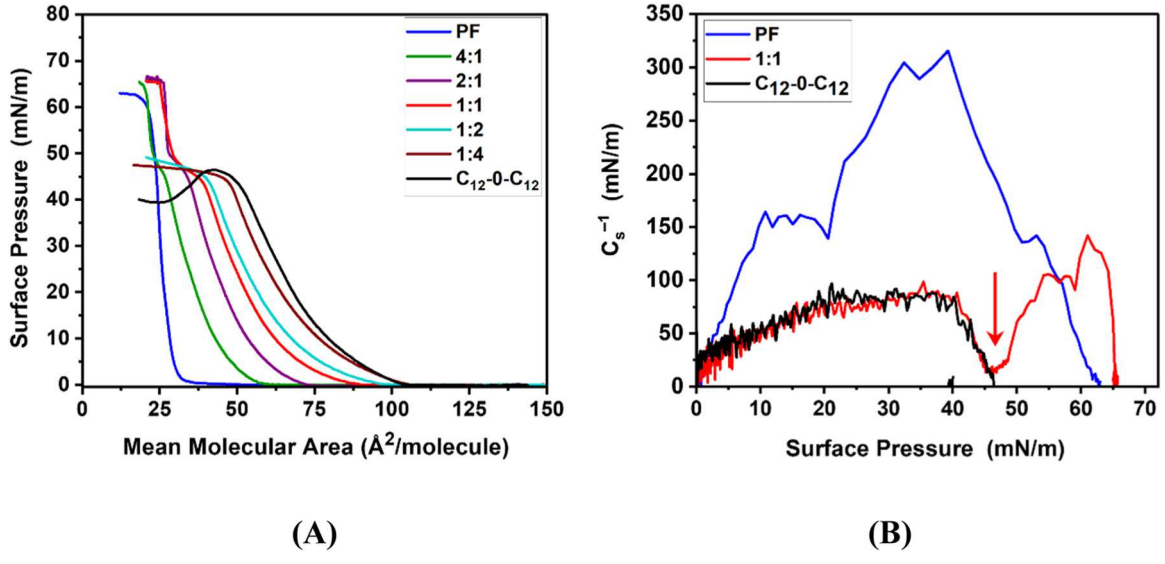

Fig. 3. **(A)** Isotherms and **(B)** compressibility modulus plots of pure and mixed PF−C_{12}-0-C_{12} films.

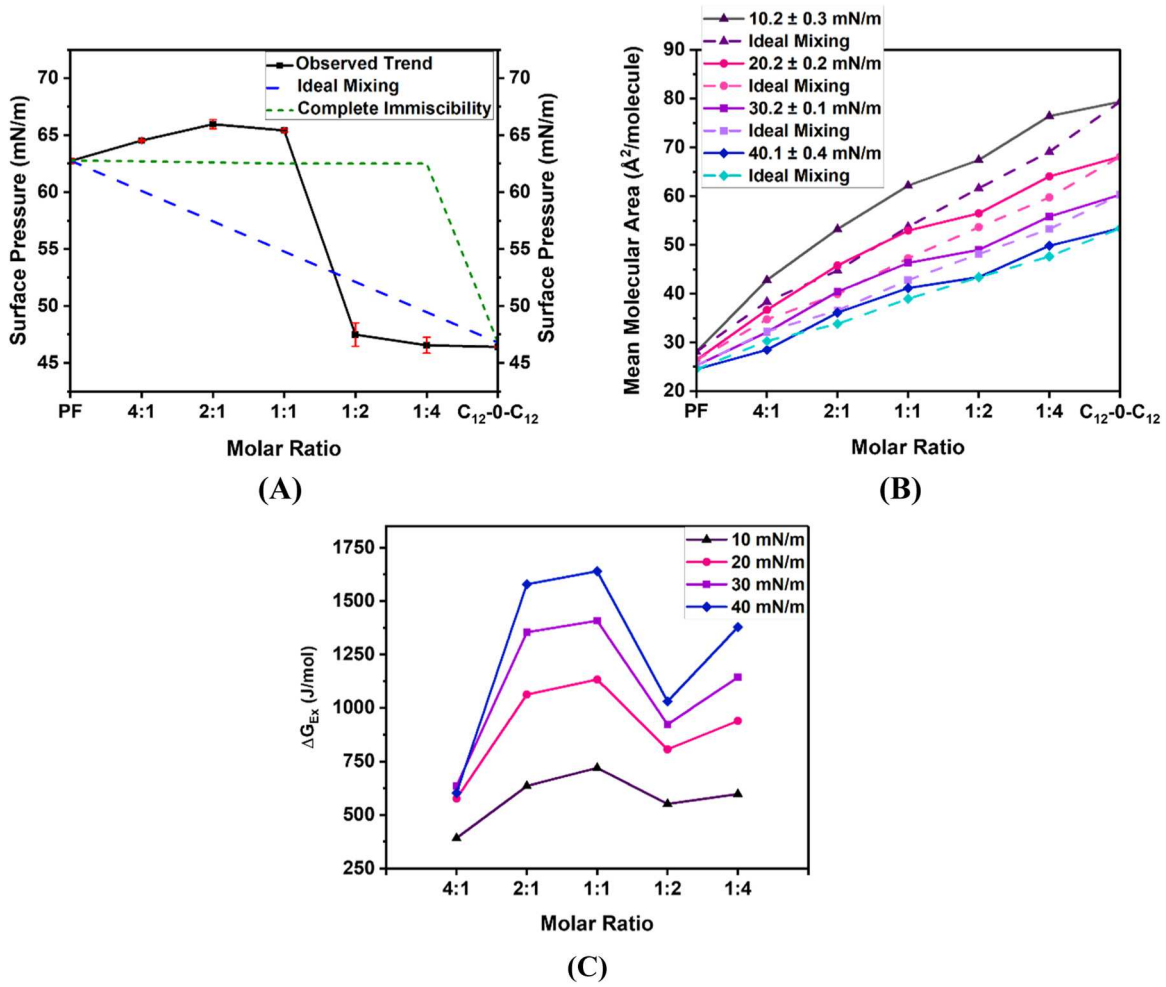

Fig. 4. **(A)** Defay-Crisp plot **(B)** additivity plots and, **(C)** plot showing excess Gibbs free energy of mixing for different mole ratios of PF—C_{12}-0-C_{12} mixed systems.

(for 4:1 at 10 mN/m) to 1640 J·mol^{-1} (for 1:1 at 40 mN/m). The magnitude of the positive ΔG_{ex} values, indicative of repulsive forces between the two components, increases with increasing surface pressure for all compositions, but the most for 2:1 and 1:1 mixtures. Albeit speculative, we postulate that the increasing repulsive forces at higher surface pressures for these mixtures facilitate the squeeze-out of C_{12}-0-C_{12} into the subphase at its collapse plateau observed around ~ 45 mN/m (see isotherms for 2:1, 1:1 mixtures).

The isotherms for the mixed PF:C_{16}-0-C_{16} monolayers fell between the isotherms for the pure individual component films. The lift-off

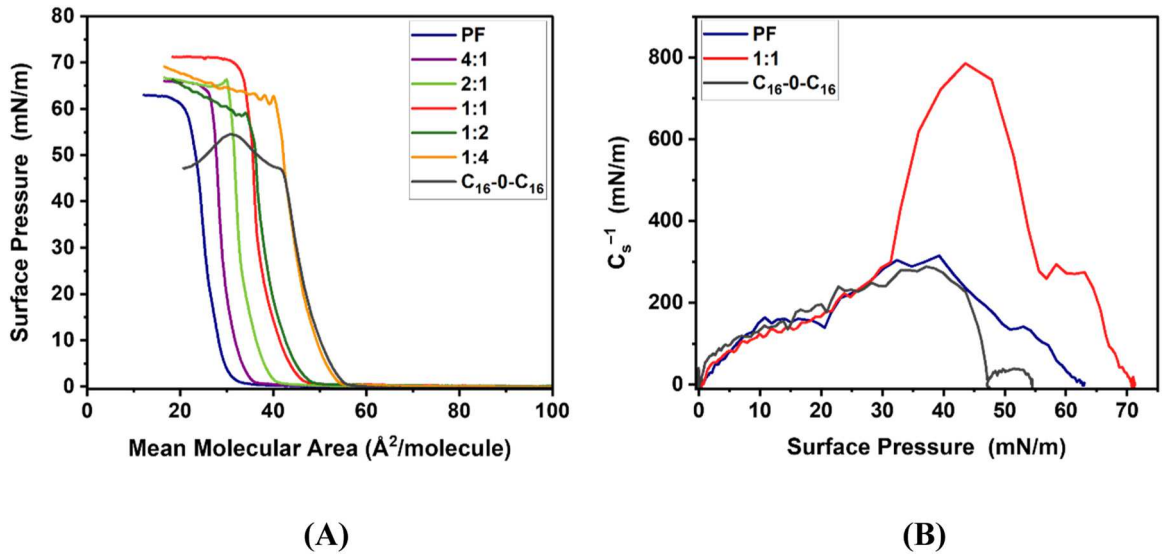

Fig. 5. **(A)** Isotherms and **(B)** compressibility modulus plots of pure and mixed PF−C_{16}-0-C_{16} films.

MMAs for different compositions shift from lower to higher MMAs going from PF to C_{16}-0-C_{16} films (Fig. 5 A), indicating that the mixed films become more expanded as the C_{16}-0-C_{16} content in the mixture increases.

Compressibility modulus plots ($C_s^{-1} = -A(d\pi/dA)_T$ vs π) for the pure components and a representative mixed film (1:1) are shown in Fig. 5B, with data for the rest of the mixed films included in SI, Figure S3. The mixture films have an unusually high $C_{s\,max}^{-1}$ values (~600–800 mN/m), making them more incompressible than either of the pure component films but also more than films formed by any of the members of the C_n-0-C_n series that have been reported to date.

From a comparison point of view, unlike the PF—C_{12}-0-C_{12} system, there is no phase transition observed near to the collapse pressure of either of the components in the mixture films and the collapse pressures of all mixture films resemble the collapse pressure of only one of the components, PF. The behavior represents a scenario which is close to complete immiscibility as predicted by the Defay-Crisp analysis. However, considering the uncertainties in the determination of the collapse pressures, the Defay-Crisp plot (SI, Figure S4) shows a behavior suggesting non-ideal mixing.

The additivity plot for the PF—C_{16}-0-C_{16} system also shows similar trends as that observed for the PF—C_{12}-0-C_{12} system. The experimental data showed positive deviations from ideal mixing, indicating net repulsive interactions between the film components. However, the extent of the positive deviations from the ideal mixing lines for this system were generally smaller. The maximum positive deviation observed for the PF—C_{16}-0-C_{16} system (~ 9.0 % for 1:4 mixture at $\pi = \sim$ 40 mN/m) is less than the PF—C_{12}-0-C_{12} system (19.1 % for 2:1 mixture at $\pi = \sim$ 10 mN/m). The overall repulsive interactions being less in the PF—C_{16}-0-C_{16} system is a result of higher attractive interactions in the longer tail-chains of C_{16}-0-C_{16}. Furthermore, the extent of the positive deviations (or repulsive interactions) decreases with decreasing C_{16}-0-C_{16} content such that for the 4:1 mixture (highest PF content), the components approach ideal mixing for $\pi \geq 20$ mN/m.

To compare the relative degree of film expansion that addition of the perfluorocarbon has upon C_{12}-0-C_{12} and C_{16}-0-C_{16} films, we have computed the difference in film expansion for the two sets of mixed films, reported here as Δ ($\Delta A_{10\text{-}40}$) values, defined here as:

$$\Delta \quad (\Delta A_{10-40}) = \Delta A_{10} - \Delta A_{40} \tag{4}$$

where $\Delta A_X = |\Delta A_{observed} - \Delta A_{ideal}| at X mN/m$

The Δ ($\Delta A_{10\text{-}40}$) values plotted against mixture composition (Fig. 6 C) show that under all conditions, the PF—C_{12}-0-C_{12} mixed systems expanded significantly more than the corresponding PF—C_{16}-0-C_{16} systems, a trend which was largely invariant with composition. Thus, it is clear that the PF—C_{12}-0-C_{12} films changed more with pressure than the PF—C_{16}-0-C_{16} films.

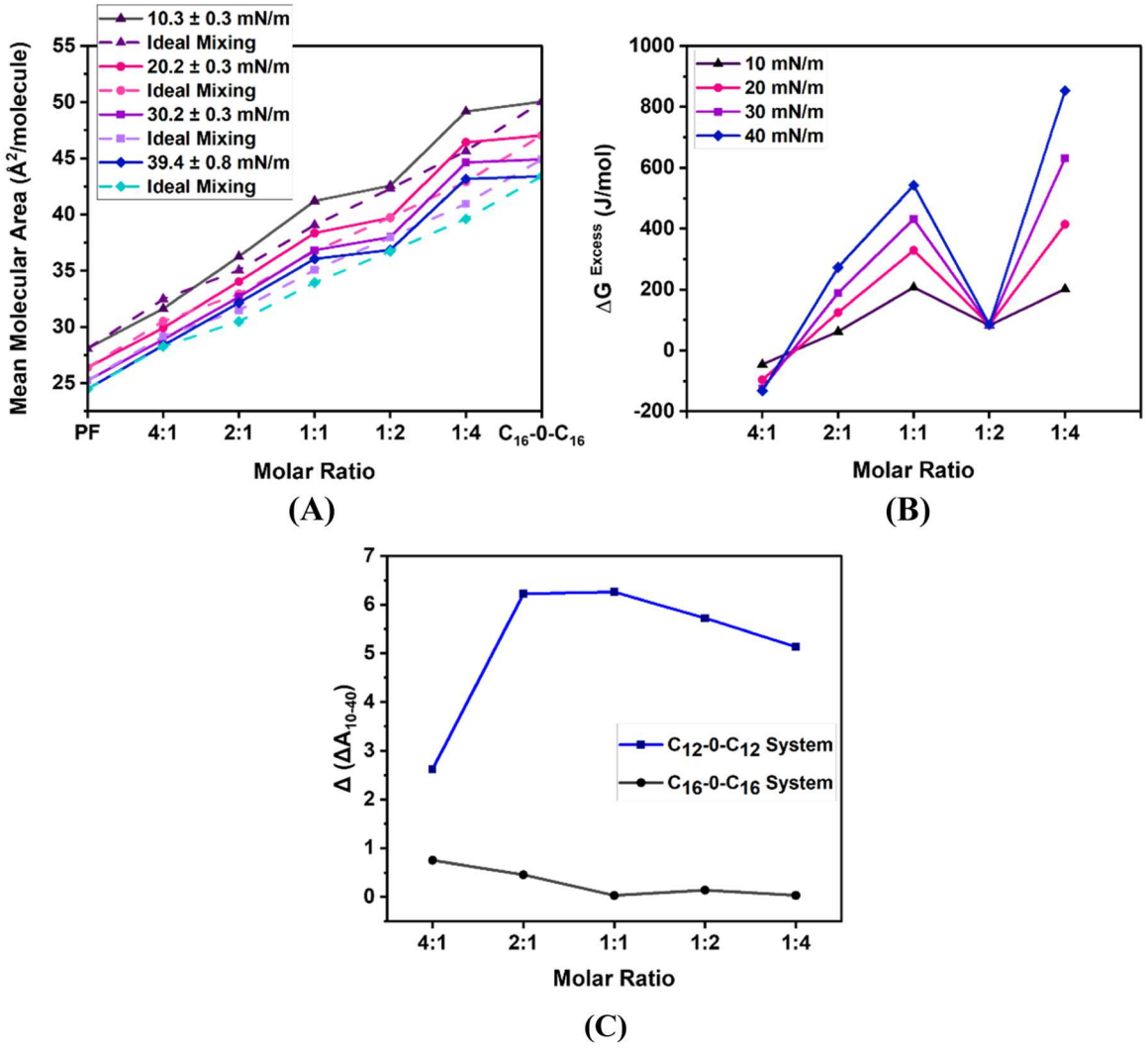

Fig. 6. **(A)** Additivity plots, **(B)** plot showing excess Gibbs free energy of mixing for different mole ratios of PF—C_{16}-0-C_{16} mixture systems, **(C)** Δ ($\Delta A_{10\text{-}40}$) values for PF—C_n-0-C_n systems.

3.2. Bulk film morphology

To elucidate the effect of mixing with PF on the two different gemini surfactants, films were characterized with BAM imaging at the air-water interface. BAM images of the monolayer films were collected over a range of mixed film compositions and surface pressures to characterize micron-scale film morphology. We note that the refractive index of perfluorocarbons is comparable with that of water, and thus PF enriched regions of monolayers will yield low reflectivity (dark regions) in the images. Further, diffraction limits spatial resolution of our BAM system to ~ 2 μm which means that film structures can, in some cases, become unresolvable with even modest compression. As control measurements, a series of BAM images taken for the two pure C_n-0-C_n films as a function of surface pressure are shown in Figs. 7, 8.

The pure C_{12}-0-C_{12} films at the lowest surface pressures showed no discernible features, but reflective patches became visible at ≥ 10 mN/m. As films were further compressed, the appearance of a porous, web-like network structure was observed. With increasing surface pressure, the void regions in the network structures became smaller but were still discernible up to the highest film compressions, and the overall reflectivity of the features increased (e.g., Fig. 7, 20 – 25 mN/m). The latter is indicative of an increase in the overall film thickness with compression, consistent with the surface-adsorbed surfactant slowly tilting towards normal to the water surface. At the highest surface pressures (nominally the collapse pressure), complex, highly-reflective shapes were observed suggesting the formation of higher-order structures and aggregates. The porous, network structure observed here is consistent with the premise that C_{12}-0-C_{12} forms expanded, liquid-like films, and chain-chain dispersion forces are insufficient to induce significant film compaction.

The pure C_{16}-0-C_{16} films had a considerably denser morphology in comparison with pure C_{16}-0-C_{16}. With even minimal compression (π slightly greater than 0 mN/m), large patches of highly reflective film were observed. The patches contained a few "perforated" void dark regions of subphase in between. As films were further compressed, the highly-reflective regions dominated the field of view, and the size and number of the void regions decreased with compression. At π ≥ 30 mN/m, void regions could no longer be meaningfully resolved except for the occasional "pinhole" defect. We note that the C_{16}-0-C_{16} monolayer morphology was very similar to that observed for the longer tail chain variant C_{18}-0-C_{18} reported previously, [23] whereas C_{12}-0-C_{12} films were entirely different, though they bore some resemblance to the previously reported Ace[12]-2-Ace[12] films, which form highly-expanded, purely liquid-phase films. [36]

BAM images for mixed films with various PF—C_{12}-0-C_{12} ratios collected at fixed film area are shown in Fig. 9. Images at constant mean molecular area are presented instead of at a constant surface pressure to ensure that the differences we see in film structures are solely due to the composition of the film and not the degree of compression. Deconvoluting these two effects is important for a proper comparison because the isotherms shift with composition. Moreover, to highlight a logical progression of composition, BAM images for two additional mixtures (3:1 and 1:3) have been included here. Film morphologies for the mixed systems were significantly different for that of pure C_{12}-0-C_{12} films. For all compositions (except for the highest C_{12}-0-C_{12} content, 1:4 mixture), films consisted of circular, low-reflectivity regions, surrounded by high-reflectivity material. As the relative amount of PF in the films decreased, the dark, circular regions decreased in diameter and the amount of bright, reflective film in the field of view increased. We ascribe the circular regions to phase-separated regions of PF (low refractive index, as per above) in a matrix of C_{12}-0-C_{12}, and the decrease in the relative area occupied by the PF domains is the result of the decrease in total PF content. The phase separated nature of the films was distinctly visible for all compositions (except for the 1:4 mixture) and indicated that the intermolecular interactions can greatly affect the extent of compaction of hydrogenated region of the film. The addition of PF seemingly promotes better compaction of C_{12}-0-C_{12} regions of the films, which appear as the homogenous, highly-reflective regions. This suggests that the net repulsive interactions between the two different film components offsets the comparatively weaker (attractive) dispersion forces for this chain-length (n = 12), driving the formation of homogenous domains instead of the web-like network structure seen for pure C_{12}-0-C_{12} even at the highest level of compression (Fig. 7).

The corresponding BAM images for the PF—C_{16}-0-C_{16} mixed films are shown in Fig. 10. As can be seen, the mixed films had different morphologies from those observed for the C_{12}-0-C_{12}. For mixed films with a higher mole fraction of PF than C_{16}-0-C_{16}, film morphology consisted of heterogeneous, mesh-like structures. The interior low-reflectivity "holes" within the mesh-like structures were generally larger in size for the 1:4 mixture than the 1:2 mixture under comparable compression conditions, indicating that a large proportion of these regions is occupied by PF. We also note that the domain contrast was non-uniform and that the overall reflectivity of the mesh-like structures increased with increasing C_{16}-0-C_{16} content.

Several distinct brightness levels for C_{16}-0-C_{16} mesh were seen for the 2:1 film which suggests the hydrogenated regions are patchy, probably containing sub-regions that are on average, thicker than the surrounding regions (marked with yellow/red arrows; Fig. 10B-D). These local regions with a seemingly higher population of C_{16}-0-C_{16} represent a vertical orientation of these molecules. The different azimuthal tilt angles of the molecules are a result of the dispersion forces

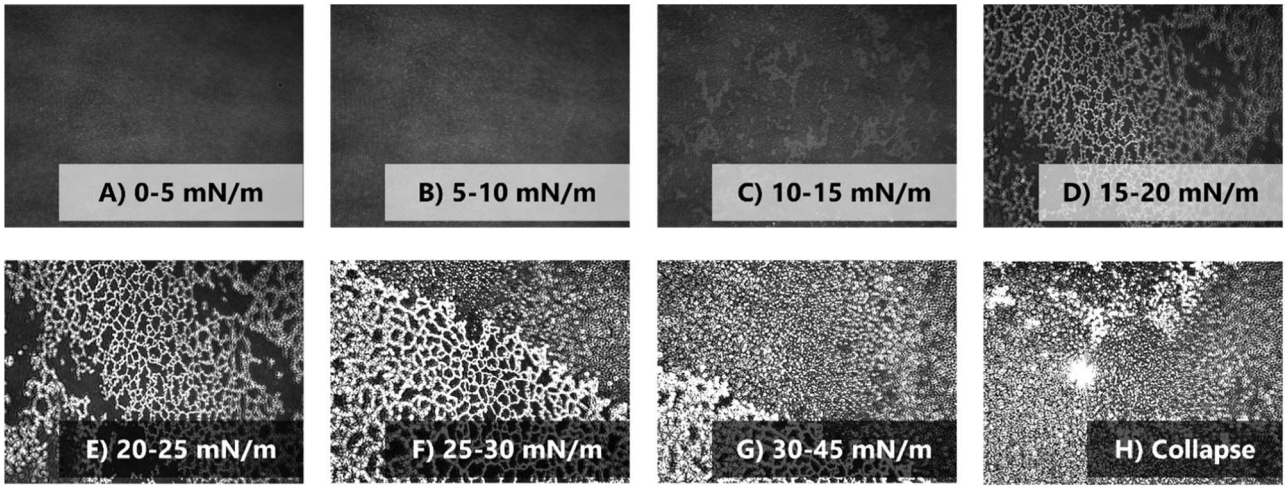

Fig. 7. Representative BAM images (696 μm × 520 μm) for pure C_{12}-0-C_{12} films as a function of surface pressure.

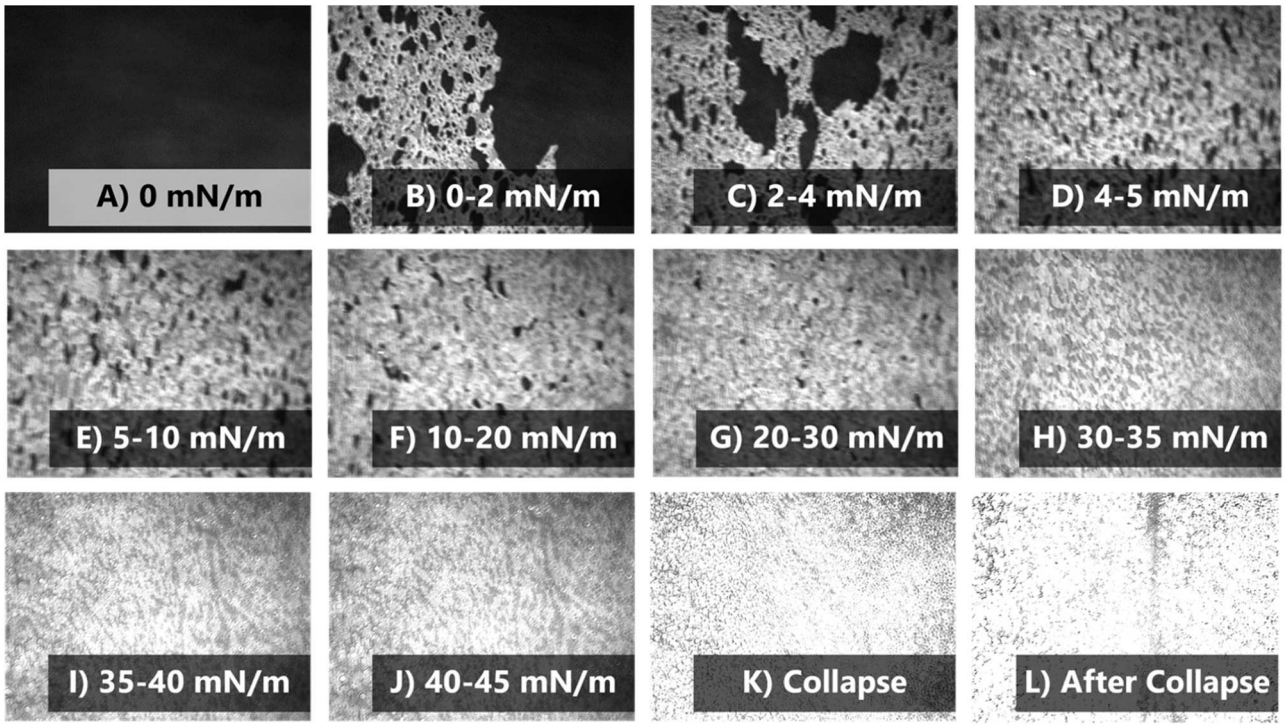

Fig. 8. Representative BAM images (696 μm × 520 μm) for pure C_{16}-0-C_{16} films as a function of surface pressure.

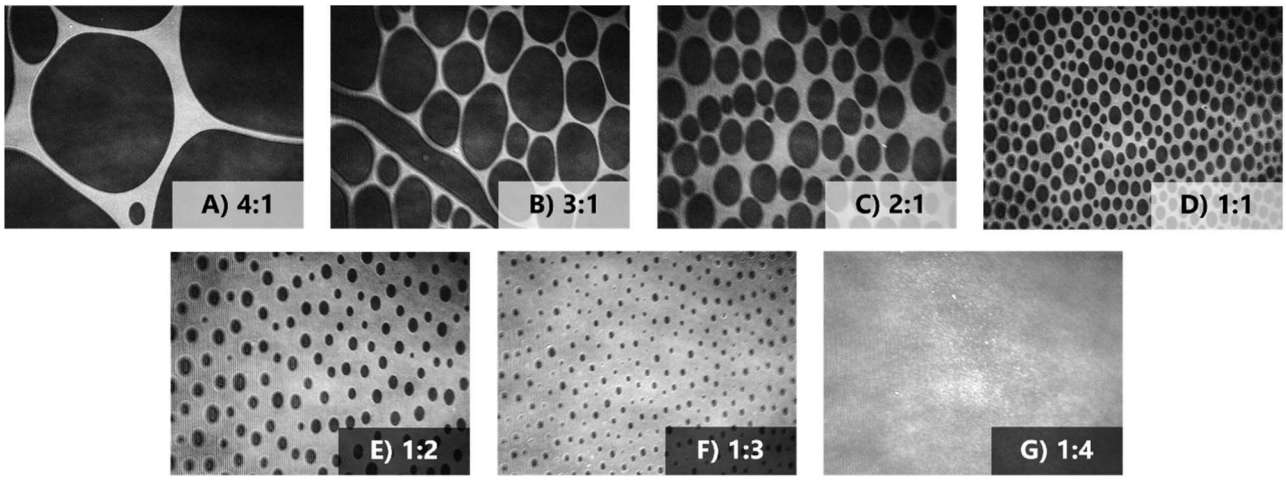

Fig. 9. Representative BAM images (696 μm × 520 μm) for pure and mixture monolayer films of PF and C_{12}-0-C_{12} at ~ 95 $Å^2$/molecule (0–5 mN/m).

that promote local clustering which pulls the molecules into a more vertical orientation (illustrated in Fig. 11). Beyond the 2:1 mixture, the highest-brightness C_{16}-0-C_{16} mesh formed by localized agglomerates of closely packed C_{16}-0-C_{16} dominate the field of view, however, the number density of these structures reasonably increases with increasing C_{16}-0-C_{16} content and thus for the 1:4 mixture, the darker holes are trapped within a matrix of C_{16}-0-C_{16}.

4. Conclusions

This study addresses the mixing behavior of dimeric-hydrogenated and monomeric-perfluorinated monolayer system constituting two tail chain variants of the C_n-0-C_n compounds. Pure C_{12}-0-C_{12} forms amorphous, liquid-like film because of the comparatively shorter tail chain and lesser resulting dispersion forces. This manifests as net-like morphological features at the micron scale. In mixed films with PF, the PF component induces closer packing of the C_{12}-0-C_{12} molecules due to the mutual immiscibility of fluorinated and hydrogenated surfactants, which makes the mixture films appear as well-separated, elliptical domains in BAM images. Although phase-separated, the extent of interactions in the PF—C_{16}-0-C_{16} mixtures is different than the PF—C_{12}-0-C_{12} system due to the differences in the attractive interactions between C_{16}-0-C_{16} and C_{12}-0-C_{12} molecules in their mixtures with PF. The observed effects provide basic knowledge of what molecular structure features of the gemini surfactant and the interactions resulting from these are needed to cause phase separation. According to our observations, a combination of repulsive interactions between a long hydrocarbon tail with a perfluorocarbon tail, as well as having a compact headgroup in the gemini surfactant are both required. Although this work provides fundamental molecular-level information on interactions in the mixed system, there are potential applications of this in controlled surface patterning in mixed hydrogenated and fluorinated systems. The

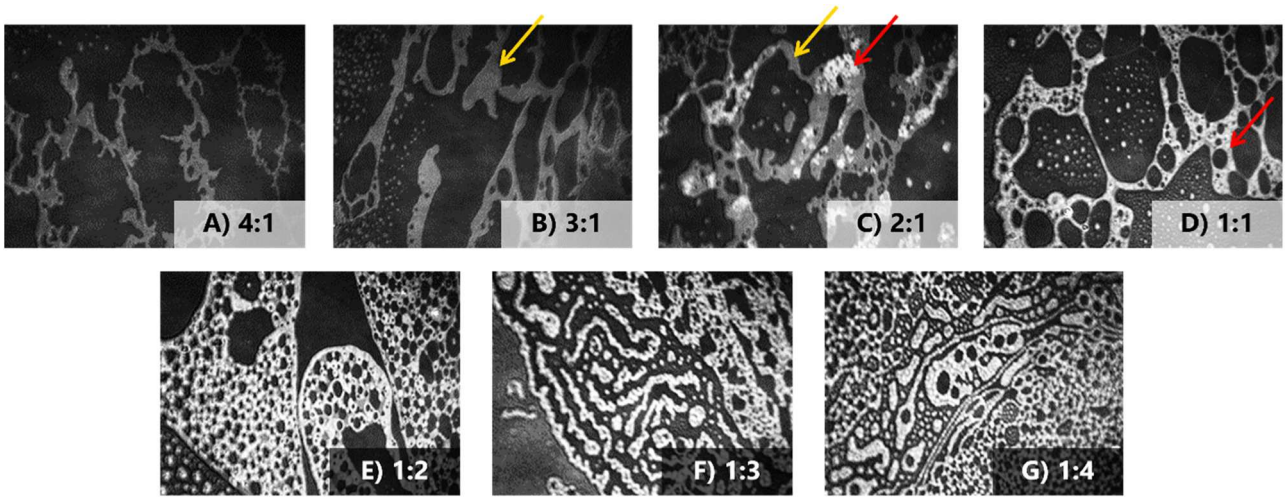

Fig. 10. Representative BAM images (696 μm × 520 μm) for pure and mixture monolayer films of PF and C_{16}-0-C_{16} at ~ 52 $Å^2$/molecule (0–5 mN/m).

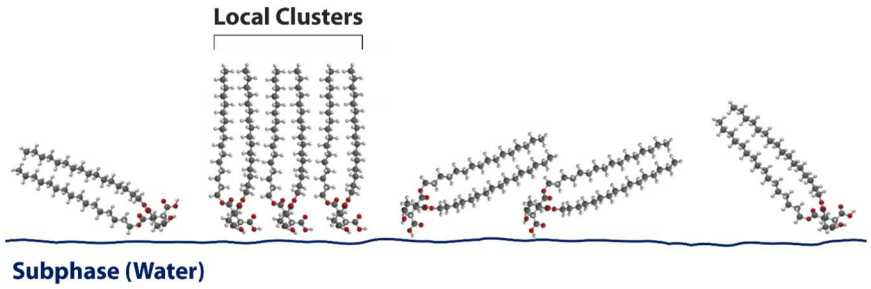

Fig. 11. Cartoon showing different possible molecular orientations and formation of local clusters of "upright" C_{16}-0-C_{16} molecules at the interface.

implications of the approach enable direct correlation of molecular structure and the resulting monolayer properties of Langmuir films at the air-water interface.

CRediT authorship contribution statement

Srikant Kumar Singh: Writing – review & editing, Writing – original draft, Investigation, Formal analysis. **Matthew Paige:** Writing – review & editing, Supervision, Project administration, Funding acquisition, Formal analysis, Conceptualization.

Declaration of Competing Interest

The authors declare that they have no known competing financial interests or personal relationships that could have appeared to influence the work reported in this paper.

Data availability

Data will be made available on request.

Acknowledgments

SKS thanks Mr. Ken-ichi Aratani and Mr. Haruyuki Mizuno (Chukyo Yushi Co. Ltd.) for supplying and Mr. Ron Johnson (Cytech Products Inc.) for facilitating the procurement of C_{12}-0-C_{12}. Financial support for this work has been provided by the Natural Sciences and Engineering Research Council, the Canadian Foundation for Innovation, and the University of Saskatchewan. NSF's ChemMatCARS, Sector 15 at the Advanced Photon Source (APS), Argonne National Laboratory (ANL) is supported by the Divisions of Chemistry (CHE) and Materials Research (DMR), National Science Foundation, under grant number NSF/CHE-1834750. This research used resources of the Advanced Photon Source, a U.S. Department of Energy (DOE) Office of Science user facility operated for the DOE Office of Science by Argonne National Laboratory under Contract No. DE-AC02–06CH11357.

Appendix A. Supporting information

Supplementary data associated with this article can be found in the online version at doi:10.1016/j.colsurfa.2024.134767.

References

[1] R. Zana, Dimeric and oligomeric surfactants. behavior at interfaces and in aqueous solution: a review, Adv. Colloid Interface Sci. *97* (1–3) (2002) 205–253, https://doi.org/10.1016/S0001-8686(01)00069-0.
[2] F.M. Menger, J.S. Keiper, Gemini surfactants, Angew. Chem. Int. Ed. *39* (11) (2000) 1906–1920, https://doi.org/10.1002/1521-3773(20000602)39:11<1906::AID-ANIE1906>3.0.CO;2-Q.
[3] S.K. Hait, S.P. Moulik, Gemini surfactants: a distinct class of self-assembling molecules, Curr. Sci. *82* (9) (2002) 1101–1112.
[4] M.J. Rosen, D.J. Tracy, Gemini surfactants, J. Surfactants Deterg. *1* (4) (1998) 547–554.
[5] M. In, R. Zana, Phase behavior of gemini surfactants, J. Dispers. Sci. Technol. *28* (1) (2007) 143–154, https://doi.org/10.1080/01932690600991888.
[6] R. Sharma, A. Kamal, M. Abdinejad, R.K. Mahajan, H.-B. Kraatz, Advances in the synthesis, molecular architectures and potential applications of gemini surfactants, Adv. Colloid Interface Sci. *248* (2017) 35–68, https://doi.org/10.1016/j.cis.2017.07.032.
[7] B.E. Brycki, I.H. Kowalczyk, A. Szulc, O. Kaczerewska, M. Pakiet, Multifunctional gemini surfactants: structure, synthesis, properties and applications, in: R. Najjar (Ed.), Application and Characterization of Surfactants, InTech, 2017, https://doi.org/10.5772/intechopen.68755.
[8] K. Sakai, H. Sakai, M. Abe, Recent advances in gemini surfactants: oleic acid-based gemini surfactants and polymerizable gemini surfactants, J. Oleo Sci. *60* (4) (2011) 159–163, https://doi.org/10.5650/jos.60.159.

[9] L. Pérez, A. Pinazo, R. Pons, Mr Infante, Gemini surfactants from natural amino acids, Adv. Colloid Interface Sci. *205* (2014) 134–155, https://doi.org/10.1016/j.cis.2013.10.020.
[10] A. Bhadani, T. Misono, S. Singh, K. Sakai, H. Sakai, M. Abe, Structural diversity, physicochemical properties and application of imidazolium surfactants: recent advances, Adv. Colloid Interface Sci. *231* (2016) 36–58, https://doi.org/10.1016/j.cis.2016.03.005.
[11] P. Tyagi, R. Tyagi, Synthesis, structural properties and applications of gemini surfactants: a review, Tenside Surfactants Deterg. *46* (6) (2009) 373–382, https://doi.org/10.3139/113.110045.
[12] M. Hossain Mondal, S. Malik, A. Roy, R. Saha, B. Saha, Modernization of surfactant chemistry in the age of gemini and bio-surfactants: a review, RSC Adv. *5* (112) (2015) 92707–92718, https://doi.org/10.1039/C5RA18462B.
[13] S.D. Wettig, R.E. Verrall, M. Foldvari, Gemini surfactants: a new family of building blocks for non-viral gene delivery systems, Curr. Gene Ther. *8* (1) (2008) 9–23, https://doi.org/10.2174/156652308783688491.
[14] F.M. Menger, V.A. Migulin, Synthesis and properties of multiarmed geminis, J. Org. Chem. *64* (24) (1999) 8916–8921, https://doi.org/10.1021/jo9912350.
[15] R. Zana, M. Benrraou, R. Rueff, Alkanediyl-.alpha.,.omega.-bis (dimethylalkylammonium bromide) surfactants. 1. effect of the spacer chain length on the critical micelle concentration and micelle ionization degree, Langmuir *7* (6) (1991) 1072–1075, https://doi.org/10.1021/la00054a008.
[16] F.M. Menger, J.S. Keiper, V. Azov, Gemini surfactants with acetylenic spacers, Langmuir *16* (5) (2000) 2062–2067, https://doi.org/10.1021/la9910576.
[17] F.M. Menger, B.N.A. Mbadugha, Gemini surfactants with a disaccharide spacer, J. Am. Chem. Soc. *123* (5) (2001) 875–885, https://doi.org/10.1021/ja0033178.
[18] R. Zana, Dimeric (Gemini) surfactants: effect of the spacer group on the association behavior in aqueous solution, J. Colloid Interface Sci. *248* (2) (2002) 203–220, https://doi.org/10.1006/jcis.2001.8104.
[19] Y. Han, Y. Wang, Aggregation behavior of gemini surfactants and their interaction with macromolecules in aqueous solution, Phys. Chem. Chem. Phys. *13* (6) (2011) 1939, https://doi.org/10.1039/c0cp01196g.
[20] Z. Jianxi, Gemini surfactants： role and significance of its spacer in self-assembly. Prog. Chem. *26* (08) (2014) 1339.
[21] Y. Gyani Devi, A. Koya Pulikkal, J. Gurung, Research progress on the synthesis of different types of gemini surfactants with a functionalized hydrophobic moiety and spacer, ChemistrySelect *7* (45) (2022) e202203485, https://doi.org/10.1002/slct.202203485.
[22] C. Yan, M.F. Paige, Pattern formation in phase-separated langmuir and langmuir monolayer films, Langmuir *37* (28) (2021) 8357–8369, https://doi.org/10.1021/acs.langmuir.1c00642.
[23] S.K. Singh, A. Yeboah, W. Bu, P. Sun, M.F. Paige, Physicochemical properties of monolayers of a gemini surfactant with a minimal-length spacer, Langmuir *38* (51) (2022) 16004–16013, https://doi.org/10.1021/acs.langmuir.2c02462.
[24] S.K. Singh, W. Bu, P. Sun, M.F. Paige, Mixing in langmuir monolayers: perfluorotetradecanoic acid and a gemini surfactant without a linker, Langmuir *39* (46) (2023) 16503–16512, https://doi.org/10.1021/acs.langmuir.3c02452.
[25] D.P. Acharya, J.M. Gutiérrez, K. Aramaki, K. Aratani, H. Kunieda, Interfacial properties and foam stability effect of novel gemini-type surfactants in aqueous solutions, J. Colloid Interface Sci. *291* (1) (2005) 236–243, https://doi.org/10.1016/j.jcis.2005.04.105.
[26] D.P. Acharya, H. Kunieda, Y. Shiba, K. Aratani, Phase and rheological behavior of novel gemini-type surfactant systems, J. Phys. Chem. B *108* (5) (2004) 1790–1797, https://doi.org/10.1021/jp036096b.
[27] S.C. Sharma, R.G. Shrestha, D. Varade, K. Aramaki, Rheological behavior of gemini-type surfactant/alkanolamide/water systems, Colloids Surf. A: Physicochem. Eng. Asp. *305* (1–3) (2007) 83–88, https://doi.org/10.1016/j.colsurfa.2007.04.044.
[28] C. Villa, S. Baldassari, D.F.C. Martino, A. Spinella, E. Caponetti, Green synthesis, molecular characterization and associative behavior of some gemini surfactants without a spacer group, Materials *6* (4) (2013) 1506–1519.
[29] G.V. Mitrofanova, V.A. Ivanova, Surface-active properties of succinic acid monoalkyl derivatives, Russ. J. Appl. Chem. *84* (3) (2011) 361–367, https://doi.org/10.1134/S1070427211030049.
[30] J.T. Davies, E.K. Rideal. Interfacial Phenomena, 2nd ed, Academic Press, New York, 1961.
[31] J. Rehman, D. Sowah-Kuma, A.L. Stevens, W. Bu, M.F. Paige, Mixing behavior in binary anionic gemini surfactant–perfluorinated fatty acid langmuir monolayers, Langmuir *33* (39) (2017) 10205–10215, https://doi.org/10.1021/acs.langmuir.7b02585.
[32] J. Rehman, D. Sowah-Kuma, A.L. Stevens, W. Bu, M.F. Paige, Immiscible anionic gemini surfactant-perfluorinated fatty acid langmuir monolayer films, Langmuir *35* (32) (2019) 10551–10560, https://doi.org/10.1021/acs.langmuir.9b01554.
[33] D. Crisp, Surface Chemistry. Supplement to Research, Butterworths, London, 1949, p. 17.
[34] Defay, R. Doctoral Dissertation, Brussels, 1932.
[35] G.L. Gaines, Insoluble Monolayers At Liquid-Gas Interfaces, Interscience Publishers, New York, 1966.
[36] J. Rehman, D. Sowah-Kuma, A.L. Stevens, W. Bu, M.F. Paige, Mixing behavior in binary anionic gemini surfactant–perfluorinated fatty acid langmuir monolayers, Langmuir *33* (39) (2017) 10205–10215, https://doi.org/10.1021/acs.langmuir.7b02585.